Plasmonics
DOI 10.1007/s11468-015-9963-9

Tuning the Plasmonic Extinction Resonances of Hexagonal Arrays of Ag Nanoparticles

Aruna Ravi [1,2] · Antriksh Luthra [1,3] · Fernando L. Teixeira [2,4] · Paul R. Berger [2] · James V. Coe [1]

Received: 7 April 2015 / Accepted: 26 April 2015

Abstract Plasmonically enhanced effects on a self-assembled, hexagonal array layer of ~4-nm silver nanoparticles are analyzed using three-dimensional finite-difference time-domain (3D FDTD) simulations and compared against experimentally measured extinction spectra. The effect of particle size, lattice spacing, and lack of monodispersity of the hexagonal array of silver nanoparticles on the extinction resonance was investigated to help determine optimal design specifications for efficient organic solar power harvesting.

Keywords Plasmon resonance · Metamaterials · Active plasmonics · Organic solar panels · Nanoparticles

Introduction

The optical properties of gold and silver nanoparticles have attracted much interest in recent years due to their potential applications in biosensors, as nano-antennas for light signal router applications and for energy transport in sub-wavelength structures, to name just a few. The localized electric field enhancement around nanoparticles interacting with incoming light also leads to a number of surface-enhanced Raman spectroscopy (SERS) applications. Myriad experimental and theoretical studies have recently been carried out to explore the potential use of nanoparticle array structures for improved nano-sensing capabilities [1–15].

An array of ~4-nm Ag nanoparticles is particularly interesting because the lattice parameter is ~100 times smaller than a probing visible wavelength. The extinction spectrum of the array has similarities to the extinction spectrum of an isolated nanoparticle. Such resonances are attributed to localized surface plasmon resonances (LSPRs); however, the array spectra are considerably affected by coupling between nanoparticles [6]. LSPRs are electron charge oscillations in metallic nanoparticles that are excited by light, and at the resonance wavelength, they exhibit enhanced, highly localized field intensity at the nanoparticle surface. Among other properties, an LSPR enables very high sub-wavelength spatial resolution as limited by the particle size, shape, and relation to neighboring particles. This work discusses plasmonically enhanced effects on hexagonal arrays of metal nanoparticles with ~4-nm Ag nanoparticles. There has also been a work on square lattice arrays [16]. Both such arrays might be useful for enhancing the efficiency of organic solar panels.

The optical absorption spectra of metal nanoparticles are dominated by LSPRs and can be tuned by changing the size, shape, particle material, substrate, and coating of the metal particles. Previously, various approaches to implementing a controlled surface plasmon-active Ag film onto organic solar cells have been introduced as random Ag nano-hole films or periodic Ag nano-cavity array [17–20]. In particular, enhanced optical absorption for polymer–fullerene bulk heterojunction PV devices, mainly due to the localized surface plasmon-enhanced photo generation of excitons through the usage of plasmon-active Ag nanospheres, has been demonstrated by Yoon et al. [21]. While electron beam lithographically prepared

✉ James V. Coe
coe.1@osu.edu

[1] Department of Chemistry and Biochemistry, The Ohio State University, Columbus, OH 43210, USA

[2] Department of Electrical and Computer Engineering, The Ohio State University, Columbus, OH 43210, USA

[3] Department of Mechanical Engineering, The Ohio State University, Columbus, OH 43210, USA

[4] ElectroScience Laboratory, The Ohio State University, Columbus, OH 43210, USA

Published online: 12 May 2015

structures have been used to study the influence of electromagnetic interactions between the particles on extinction spectra, the effect of a (inevitable) disorder due to fabrication imperfections remains an important and relatively unexplored issue [6]. Schatz and coworkers [22] investigated the effect of a disorder for a two-dimensional array with 30-nm particles and found that the interactions between particles are partially canceled by a disorder and blue-shifts in the observed plasmon resonances. Schatz and coworkers also studied the extinction spectra of silver nanoparticles in one- and two-dimensional arrays as a function of particle size and interparticle distance and found that arrays of spherical silver particles are, in some cases, capable of generating extremely narrow plasmon resonances due to an interaction between the localized plasmons in the particles and photonic states associated with the array, and that stronger coupling between particles red-shifts the plasmon peak, widens the resonance, and increases its intensity [15].

Method

Numerical methods, and especially the finite-difference time-domain (FDTD) method, are instrumental for the computation of surface plasmon resonances in complex geometrical configurations, enabling the inclusion of full interaction mechanisms between particles [23]. The FDTD method discretizes the entire problem volume using hexahedral cells and then solves the coupled Maxwell's curl equations in a marching-on-time fashion [24, 25]. In this work, plasmonically enhanced effects on a self-assembled layer of silver nanoparticles are studied by means of 3D FDTD simulations and compared against experimentally measured extinction spectra.

A self-assembled layer of silver nanoparticles (see left of Fig. 1) was simulated by using a ~4-nm diameter and ~6-nm lattice spacing. The extinction resonance is obtained at a wavelength of 465 nm, which is greater than 100 times the particle diameter. The FDTD grid utilized for the hexagonal array unit cell with Ag nanoparticles is shown schematically in Fig. 1 (middle). An electromagnetic plane-wave light source (linearly polarized along the x direction) having an effective bandwidth between wavelengths 300 and 800 nm is an incident on the unit cell, which is embedded on a quartz substrate of thickness 4 nm. A detector of size 6×10.3923 nm is positioned above the unit cell at a distance of approximately 45 nm to measure the intensity of light transmitted. The overall FDTD simulation domain is of size $6 \times 10.3923 \times 150$ nm. The FDTD algorithm includes an automatic non-uniform meshing, implements periodic boundary conditions in the x and y directions, and utilizes the perfectly matched layer (PML) [26–28] absorbing boundary condition in the z direction (direction of incident light). Figure 1 (right) shows the simulated extinction spectra (4-nm diameter, 6-nm lattice parameter, and no other adjustable parameters) compared against the experimentally measured spectra.

Effect of Size and Lattice Parameter

Numerous prior experiments have shown that the optical spectra of arrays and aggregates are influenced by particle shape, size, interactions between neighboring particles, and polarization of the incident light. When the interparticle distance is comparable to or less than the particle size, the interactions between particles play a significant role in the optical response. Initially, the effects of particle radius and periodic lattice spacing on the extinction resonance of hexagonal array of Ag nanoparticles were examined. For this purpose, the original periodic lattice (center to center) spacing was held constant while varying the particle radii in steps of 0.25 nm, starting from a radius of 1 nm (where the nearest neighbors are well apart from each other) to a radius of 2.25 nm (where they are nearly touching). The resulting extinction resonances are shown in Fig. 2a. At small particle sizes, the extinction resonance is small as much light is transmitted between particles to the detector. However, as the particle size gets larger, the extinction peak becomes more prominent, due to absorption and increased scattering of light by the particle. When the particles nearly touch each other, electromagnetic coupling between adjacent nanoparticles starts distorting the resonance lineshapes. There is also an observable shift in

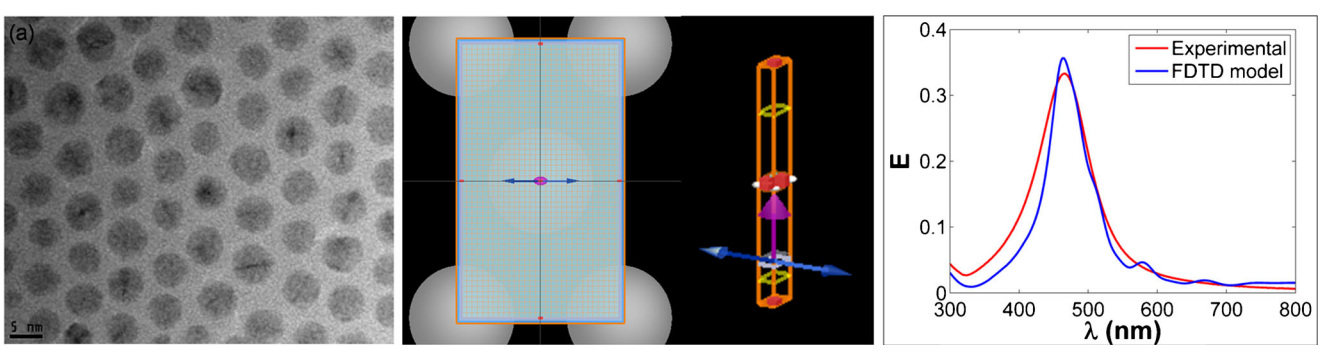

Fig. 1 At the *left* is a TEM image of experimental self-assembled Ag nanospheres with a scale bar of 5 nm, at the *center* is the FDTD setup of the hexagonal array unit cell, and at the *right* are preliminary results comparing experimental extinction spectra and FDTD results

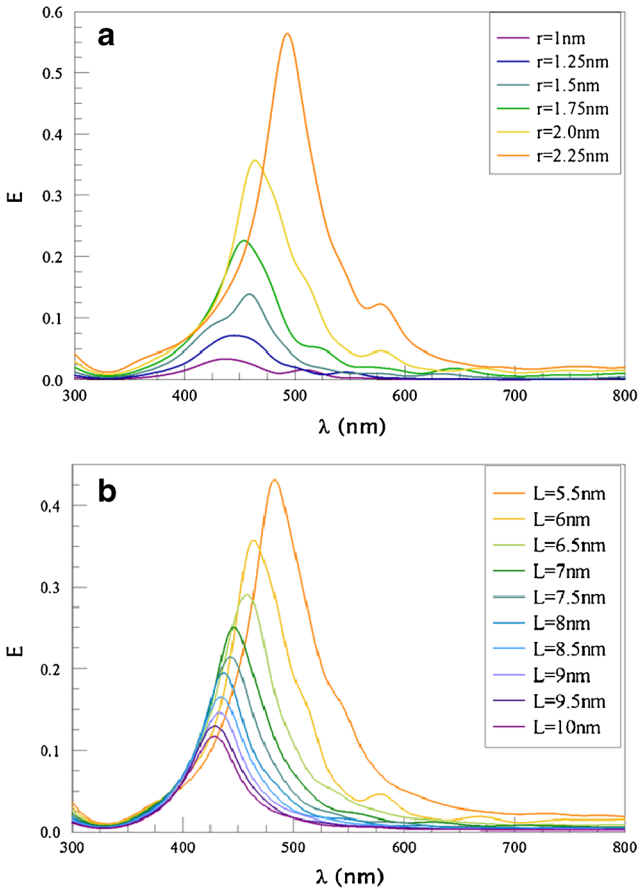

Fig. 2 Extinction spectra of hexagonal array of Ag nanoparticles. The *top* is a constant lattice spacing (6 nm), varying radius (red circles in Fig. 4). The *bottom* is a constant radius (2 nm), varying lattice spacing (green circles in Fig. 4)

resonance peaks to higher wavelengths with an increasing particle size. Next, the original particle radius of 2 nm was maintained at a constant value while the periodic lattice (center to center) spacing was varied in steps of 0.5 nm, starting with a spacing of 10 nm (where the nearest neighbors are well apart from each other) to a spacing of 5.5 nm (where they are nearly touching). The resulting extinction resonances are shown in Fig. 2b. As expected at large spacing, the extinction resonance is relatively small since most light goes between particles to the detector. As the center-to-center spacing is decreased, the particles get closer and the extinction peak becomes more prominent. When the particles nearly touch each other, electromagnetic coupling between adjacent nanoparticles distorts the resonance lineshapes. Once again, there is a noticeable shift in resonance peaks to higher wavelengths with decreasing lattice spacing.

Polydispersity

In practice, non-ideal fabrication processes result in arrays that exhibit distributions in both lattice spacing and radii, as visible in Fig. 1 (TEM image on the left). The effects of such variations in radii and lattice spacing on resonances can be studied by assuming a Gaussian probability distribution function for such parameters. Using the software package ImageJ (http://imagej.nih.gov/ij/), the aforementioned TEM image was analyzed and a binary image was created to produce a distinct contrast between the Ag nanospheres and the quartz background, as shown in Fig. 3. Plots were made of the individual particle radii vs. the corresponding particle-center-to-particle-center values showing Gaussian distributions of these properties and a slight (smaller than the distribution widths)

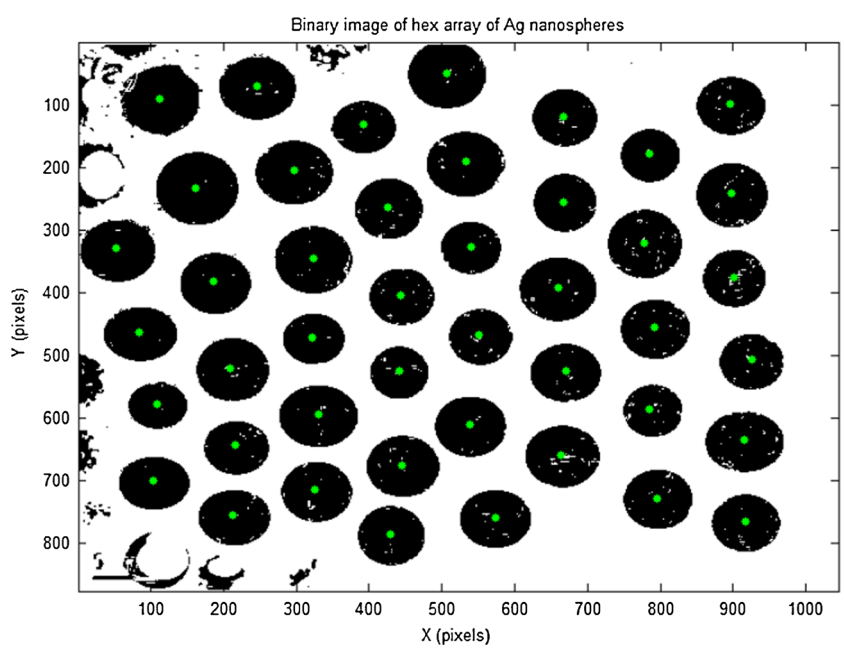

Fig. 3 Binary image of self-assembled hex array of Ag nanospheres and their center points

correlation between radii and lattice parameter. A grid of radii and lattice parameters was chosen (see Fig. 4, black dots) to match the range of experimental variations in Fig. 3. The tilt of the grid lines indicates the observed correlation between a radius and lattice parameter as reflected in the experimental data. FDTD simulations were performed at the radii and lattice spacings of the black dots in Fig. 4 in order to understand the impact of the experimental distributions in radii and lattice spacing, i.e., to ascertain the effects of a lack of monodispersity in a practical fabrication process on resonances. The extinction spectra of a related set (blue circles about black dots in Fig. 4) are presented in Fig. 5. This set constrains the radius (R_i) to a value of the lattice parameter (L_i) by $R_i = 0.02757L_i + 2.0089$, where both R_i and L_i are in units of nanometer. This set of spectra nicely spans the region about the observed experimental extinction spectrum.

Fitting Extinction Spectra of Uniform Lattices over Range of Size and Lattice Parameters

The FDTD extinction spectra (E_j) from a grid of R_i, L_i values (black dots in Fig. 4) were fitted to a Lorentzian lineshape using the following equation:

$$E_j = \frac{H}{1 + \left(\frac{\lambda_j - P}{w}\right)^2} + c \tag{1}$$

where j is an index for wavelength, λ_j is the wavelength, H is the peak height or intensity, P is the peak position, w is the half-width-at-half-max, and c is an offset parameter. An example of such a fit is shown in Fig. 6. Fits were also performed vs. wavenumber, i.e., the reciprocal of wavelength which is

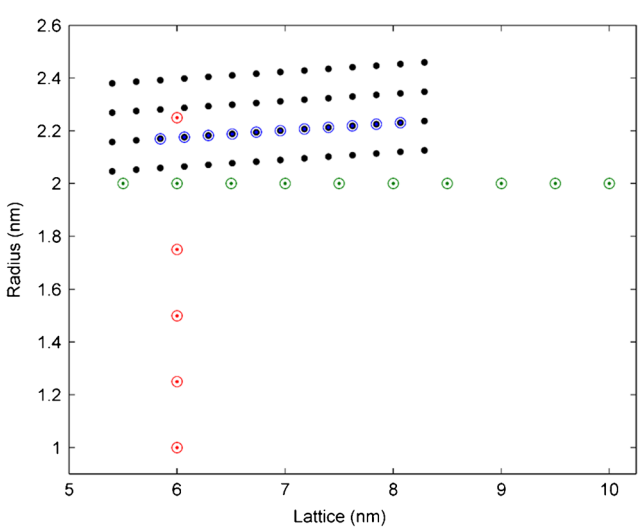

Fig. 4 FDTD data points (*small black dots*), constant lattice spacing (*red circles*), constant particle radius (*green circles*); varying particle radius, varying lattice spacing (*blue circles*)

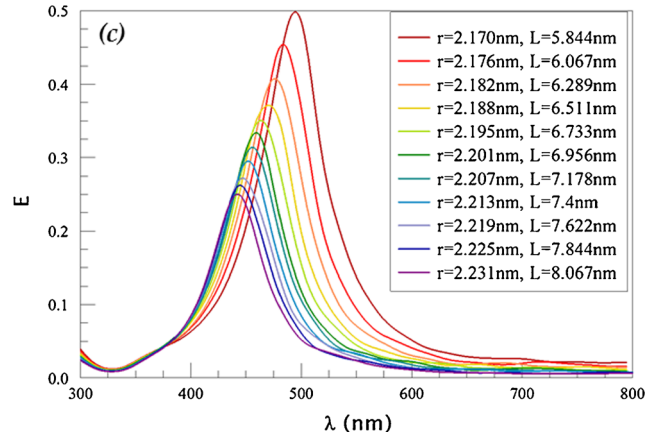

Fig. 5 Extinction spectra of hexagonal array of Ag nanoparticles. Varying particle radius, varying lattice spacing (blue circles in Fig. 4)

proportional to energy where a Lorentian lineshape is expected to be more appropriate; however, the Lorentzian wavelength fits were better in all cases examined. Fits were obtained for the extinction spectra of all of the black dots in Fig. 4, and the results have been presented in Table 1.

The fitted extinction lineshapes were then used to generate 3D scatter plots (blue symbols in Fig. 7) for various radii (R_i) and lattice parameters (L_i) vs. the extinction peak positions, P_i (top of Fig. 7); peak heights, H_i (middle of Fig. 7); and peak full-width-at-half-max, W_i ($2w_i$, bottom of Fig. 7), where i is an index over the FDTD data points (black symbols) in Fig. 4. The following multiple linear regression equations give the surface fits in Fig. 7:

$$P_i = 534.7R_i - 82.05L_iR_i + 6.341L_i^2 + 2.166L_i^2R_i \tag{2}$$

$$H_i = 1.233R_i - 0.2427L_iR_i - 0.01648L_i^2 + 0.02010L_i^2R_i \tag{3}$$

$$W_i = 96.52R_i - 18.04L_iR_i + 0.8457L_i^2 + 0.8100L_i^2R_i \tag{4}$$

where R_i, L_i, P_i and W_i are in units of nanometer and H_i is unitless (extinction). The standard deviations of the fits are

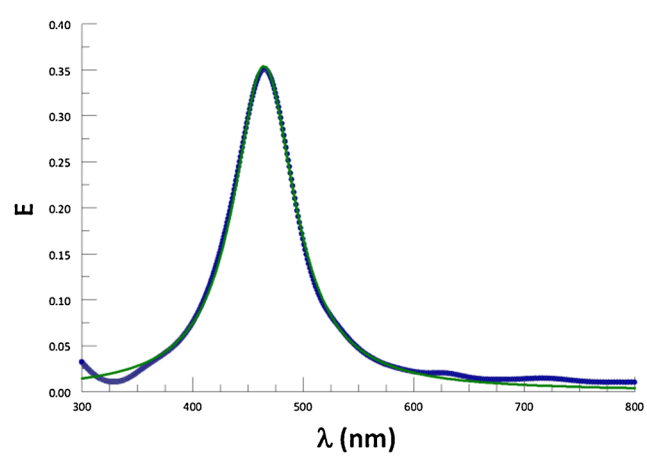

Fig. 6 Example of FDTD model extinction spectra (in *blue*) fitted to a Lorentzian lineshape (in *green*). The best fit parameters were $H = 0.354(10)$, $w = 33.3(20)$, $P = 464.72(10)$, and $c = 0.00(0)$

Table 1 The peak positions (P), peak heights (H), and peak widths (W) as full-widths-at-half-maximum for various values of nanoparticle radius (R) and nanoparticle array lattice parameter (L)

L (nm)	R (nm)	P (nm)	H	W (nm)
5.622	2.386	544.218	0.8039	68.8227
5.844	2.392	526.316	0.7165	69.5661
6.067	2.398	509.554	0.6713	63.8832
6.289	2.405	509.554	0.6713	63.8832
6.511	2.411	486.815	0.5624	61.5717
6.733	2.417	479.042	0.5103	62.6355
6.956	2.423	470.588	0.47	61.3198
7.178	2.429	465.116	0.4379	61.0572
7.4	2.435	458.891	0.4076	59.9153
7.622	2.441	457.143	0.3531	68.0457
7.844	2.447	451.977	0.3252	69.1147
8.067	2.453	448.598	0.3187	65.2761
8.289	2.46	446.097	0.2909	67.9499
5.4	2.269	542.986	0.7836	66.483
5.622	2.275	525.164	0.5813	88.078
5.844	2.281	509.554	0.5509	79.0054
6.067	2.287	495.868	0.4976	78.0704
6.289	2.293	486.815	0.4753	71.7588
6.511	2.3	478.088	0.4256	74.026
6.733	2.306	471.513	0.4084	68.8125
6.956	2.312	465.116	0.3635	72.2919
7.178	2.318	459.77	0.3568	66.2658
7.4	2.324	456.274	0.3249	68.3073
7.622	2.33	451.977	0.3169	64.234
7.844	2.336	448.598	0.297	63.7947
8.067	2.342	445.269	0.2899	60.7521
8.289	2.348	442.804	0.266	62.7137
5.4	2.158	516.129	0.5875	73.3402
5.622	2.164	505.263	0.5512	69.3015
5.844	2.17	494.845	0.4932	70.3048
6.067	2.176	484.848	0.4506	69.1059
6.289	2.182	477.137	0.41	69.2686
6.511	2.188	470.588	0.38	67.929
6.733	2.195	465.116	0.3543	66.7495
6.956	2.201	459.77	0.334	64.2519
7.178	2.207	455.408	0.315	63.2183
7.4	2.213	451.128	0.2959	62.1791
7.622	2.219	447.761	0.2751	63.1247
7.844	2.225	445.269	0.264	61.1559
8.067	2.231	441.989	0.2515	59.4764
8.289	2.237	440.367	0.2369	60.3606
5.4	2.047	503.145	0.4716	77.3067
5.622	2.053	491.803	0.4571	69.102
5.844	2.059	481.928	0.416	67.2232
6.067	2.065	475.248	0.3873	65.7546
6.289	2.071	467.836	0.3664	61.1733
6.511	2.077	463.32	0.3391	61.4857
6.733	2.083	458.015	0.3198	58.6576
6.956	2.089	453.686	0.296	59.2172
7.178	2.096	449.438	0.2772	58.3537
7.4	2.102	446.927	0.2614	58.0286
7.622	2.108	444.444	0.2333	63.5007
7.844	2.114	441.176	0.218	63.9481
8.067	2.12	440.367	0.2056	64.5887
8.289	2.126	437.956	0.1953	64.2689

2.8, 0.045, and 4.7 nm for P_i, H_i, and W_i, respectively. The variance-covariance matrix shows that there are correlations between the independent variables, but this particular choice of independent variables has less correlation between variables than all others that were tried. Equations 2–4 allow one to predict the position, height, and width of the extinction resonance for hexagonal Ag nanoparticle arrays with $2.047\,nm \leq R_i \leq 2.46\,nm$ and $5.4\,nm \leq L_i \leq 8.29\,nm$. The surfaces are not reliable outside of these ranges.

Coupling effects are the smallest when L is large and R is small, i.e., the right-hand side of the plots in Fig. 7. All of the

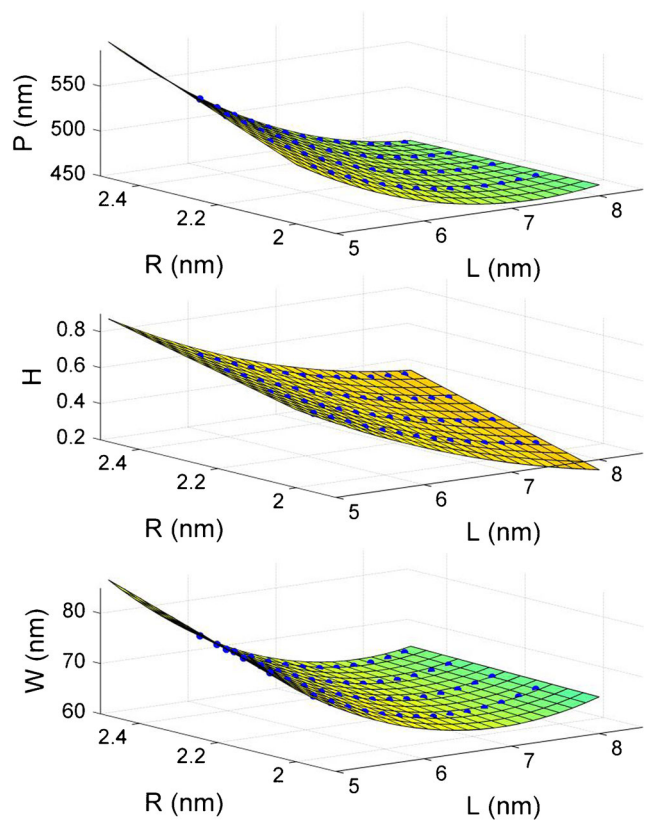

Fig. 7 Surface plots: R vs. L vs. peak position (P, *top*), peak height (H, *center*), and FWHM (W, *bottom*). Multiple linear regression fits for the surfaces are given in Eqs. 2–4

surfaces of Fig. 7 increase to the left-hand side, where L is small and R is big, i.e., strong coupling. Strong coupling correlates with red-shifted peaks, more intense peaks, and wider peaks. The peak widths, W (or FWHM) relate inversely to the lifetimes of resonances, so a particular application might vary L and R to obtain the narrowest resonance and the most intense peak for a desired wavelength. Narrower resonances work better for solar panel design as a strong interaction of nanoparticles with light provides efficient absorption in the active layer and increases overall efficiency of the solar cell [29, 30]. These surface plots provide an excellent physical insight to help determine specifications for optimal nanoparticle radii and lattice spacing to increase absorption in solar cells. Trends can be extracted from the fits of Eqs. 2–4. For example, consider the specific example of $R = 2.201\,nm$ and $L = 6.956\,nm$. The linear change in a peak position with a radius dominates with $\frac{\partial \mathrm{P}}{\partial \mathrm{R}} = 68.8$ and $\frac{\partial \mathrm{P}}{\partial \mathrm{L}} = -26.1$ in units of nanometer of wavelength shift per nanometer of nanoparticle radius or lattice parameter, respectively. Likewise, the linear trends in widths dominate and are $\frac{\partial \mathrm{W}}{\partial \mathrm{R}} = 10.2$ and $\frac{\partial \mathrm{W}}{\partial \mathrm{L}} = -3.1$ in units of nanometer of width per nanometer of nanoparticle radius or lattice parameter, respectively. However, changes in peak height with either R or L are more complicated and not dominated by linear terms. Both change sign over the range considered, so specific values of R and L must be considered.

Effect of Polydispersity on Extinction Spectra

The widths of these extinction resonances are an interesting topic. If one tries to match the experimental extinction spectrum by varying L and R of a homogeneous array, the predicted spectra are always narrower (see right of Fig. 1). For nanoparticles of this small size, it is known that the permittivity can change from the bulk value as a function of particle radius [31]. However, any practical fabrication process will suffer from polydispersity, i.e., a distribution in particle sizes. It is clear from the TEM image (left of Fig. 1) that there is a distribution in particle size and lattice spacing due to the commercial non-ideal fabrication process. To address the lack of monodispersity, additional 3D FDTD simulations were performed using a larger, non-uniform hexagonal array unit cell (top left of Fig. 8). While the earlier simulation involved two nanoparticles per cell, this simulation involved 36 particles per cell. This simulation started with the positions of nanoparticles in the experimental image (Fig. 3), to which were added

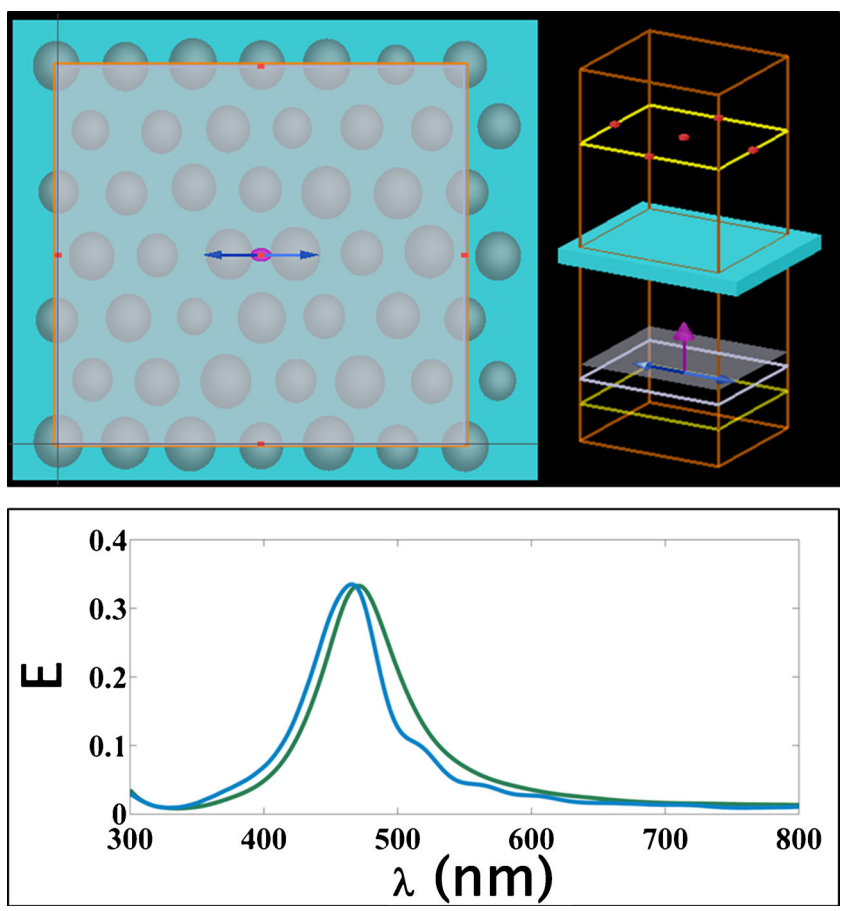

Fig. 8 The t*op* is a FDTD setup of hex array of Ag nanoparticles with a larger, non-uniform unit cell. The *bottom* is a comparison of FDTD extinction spectra *E*: non-uniform hexagonal array model (*green curve*) vs. uniform periodic hexagonal array model (*blue curve*)

variations in radius and spacing between particles from random Gaussian deviates and distribution input values of 2.0±0.177 nm for the mean and standard deviation of particle radius and 5.95±0.119 nm for the mean and standard deviation of lattice parameter. The new pattern of Ag nanoparticles (top left of Fig. 8) arising from the assumed distributions was embedded in a host substrate having an average dielectric index of 1.55. Note that in the original experiment, the self-assembled Ag nanoparticles were formed between the indium–tin oxide (ITO) coated glass substrate and poly(3,4-ethylenedioxythiophene)-poly(styrenesulfonate) (PEDOT:PSS) along with a photoactive layer of poly(3-hexylthiophene) (P3HT) and [6, 6]-phenyl-C61-butyric acid methyl ester (PCBM) blend film [21]. The extinction spectrum results are shown in Fig. 8 where the 36 particle patterns with variations patterns with variations are compared to that of a two-particle homogeneous array. The extinction spectra obtained using the homogeneous array are narrower and have additional higher order modes that arise due to the symmetry of the periodic hexagonal array. The 36 particle patterns with variations better emulate the lineshape of the original experimental extinction spectrum, both in its smoothness and width.

Conclusion

The 3D FDTD method captures the spectral behavior of hexagonal arrays of small (~4 nm) Ag nanoparticles that are ~100 times smaller than the probing wavelength. The resulting extinction spectra resemble the spectra of isolated Ag nanoparticles, except that there are shifts and increases of width and intensity due to coupling between particles in the lattice. At first, the results from uniform arrays at varying radii and lattice parameter were compared to the experimental extinction spectrum of a self-assembled hexagonal array of Ag nanoparticles with an unavoidable distribution of sizes and lattice parameters. The simulated spectra were always narrower and more structured, so a polydisperse system was modeled with a distribution of radii and lattice parameters. Polydispersity is clearly capable of explaining the breath and smoothness of the experimental spectrum which unfortunately obscures the ability to look at other effects, such as change of the permittivity of small nanoparticles from bulk. In the future, it would be very interesting to do such experiments and simulations on arrays with narrower size distributions where polydispersity does not dominate.

Acknowledgments We thank the National Science Foundation for the support of this work under Grant No. ECCS-1202465. The FDTD code utilized is provided by Lumerical Solutions Inc., Vancouver, BC, Canada. ImageJ and its Java source code are in the public domain and are freely available from the National Institutes of Health.

References

1. Boal AK, Ilhan F, DeRouchey JE, Thurn-Albrecht T, Russell TP, Rotello VM (2000) Self-assembly of nanoparticles into structured spherical and network aggregates. Nature (London) 404(6779): 746–748
2. Brongersma ML, Polman A, Min KS, Boer E, Tambo T, Atwater HA (1998) Tuning the emission wavelength of Si nanocrystals in SiO2 by oxidation. Appl Phys Lett 72(20):2577–2579. doi:10.1063/1.121423
3. Elghanian R, Storhoff JJ, Mucic RC, Letsinger RL, Mirkin CA (1997) Selective colorimetric detection of polynucleotides based on the distance-dependent optical properties of gold nanoparticles. Science (Washington, D C) 277(5329):1078–1080. doi:10.1126/science.277.5329.1078
4. Fleischmann M, Hendra PJ, McQuillan AJ (1974) Raman spectra of pyridine adsorbed at a silver electrode. Chem Phys Lett 26(2): 163–166. doi:10.1016/0009-2614(74)85388-1
5. Haes AJ, Zou S, Schatz GC, Van Duyne RP (2004) Nanoscale optical biosensor: short range distance dependence of the localized surface plasmon resonance of noble metal nanoparticles. J Phys Chem B 108(22):6961–6968. doi:10.1021/jp036261n
6. Haynes CL, McFarland AD, Zhao L, Van Duyne RP, Schatz GC, Gunnarsson L, Prikulis J, Kasemo B, Kaell M (2003) Nanoparticle optics: the importance of radiative dipole coupling in two-dimensional nanoparticle arrays. J Phys Chem B 107(30):7337–7342. doi:10.1021/jp034234r
7. Jeanmaire DL, Van Duyne RP (1977) Surface Raman spectroelectrochemistry. Part I. Heterocyclic, aromatic, and aliphatic amines adsorbed on the anodized silver electrode. J Electroanal Chem Interfacial Electrochem 84(1):1–20. doi:10.1016/0368-1874(77)80399-7
8. Krenn JR, Schider G, Rechberger W, Lamprecht B, Leitner A, Aussenegg FR, Weeber JC (2000) Design of multipolar plasmon excitations in silver nanoparticles. Appl Phys Lett 77(21):3379–3381. doi:10.1063/1.1327615
9. Malynych S, Chumanov G (2003) Light-induced coherent interactions between silver nanoparticles in two-dimensional arrays. J Am Chem Soc 125(10):2896–2898
10. Mirkin CA, Letsinger RL, Mucic RC, Storhoff JJ (1996) A DNA-based method for rationally assembling nanoparticles into macroscopic materials. Nature 382(6592):607–609
11. Nie S, Emory SR (1997) Probing single molecules and single nanoparticles by surface-enhanced Raman scattering. Science (Washington, D C) 275(5303):1102–1106. doi:10.1126/science.275.5303.1102
12. Oldenburg SJ, Hale GD, Jackson JB, Halas NJ (1999) Light scattering from dipole and quadrupole nanoshell antennas. Appl Phys Lett 75(8):1063–1065. doi:10.1063/1.124597
13. Storhoff JJ, Elghanian R, Mucic RC, Mirkin CA, Letsinger RL (1998) One-pot colorimetric differentiation of polynucleotides with single base imperfections using gold nanoparticle probes. J Am Chem Soc 120(9):1959–1964. doi:10.1021/JA972332I
14. Van Duyne RP, Hulteen JC, Treichel DA (1993) Atomic force microscopy and surface-enhanced Raman spectroscopy. I. Silver island films and silver film over polymer nanosphere surfaces supported on glass. J Chem Phys 99(3):2101–2115. doi:10.1063/1.465276
15. Zou S, Janel N, Schatz GC (2004) Silver nanoparticle array structures that produce remarkably narrow plasmon lineshapes. J Chem Phys 120(23):10871–10875
16. Sun C, Wang X (2015) Efficient light trapping structures of thin film silicon solar cells based on silver nanoparticle arrays. Plasmonics 10(37). doi:10.1007/s11468-015-9934-1

17. Barnes WL, Dereux A, Ebbesen TW (2003) Surface plasmon subwavelength optics. Nature (London) 424(6950):824–830. doi:10.1038/nature01937
18. Mock JJ, Barbic M, Smith DR, Schultz DA, Schultz S (2002) Shape effects in plasmon resonance of individual colloidal silver nanoparticles. J Chem Phys 116(15):6755–6759. doi:10.1063/1.1462610
19. Royer P, Goudonnet JP, Warmack RJ, Ferrell TL (1987) Substrate effects on surface-plasmon spectra in metal-island films. Phys Rev B Condens Matter 35(8, Pt. 1):3753–3759
20. Jin P, Xu G, Tazawa M, Yoshimura K (2003) Design, formation and characterization of a novel multifunctional window with VO2 and TiO2 coatings. Appl Phys A Mater Sci Process 77(3–4):455–459. doi:10.1007/s00339-002-1460-2
21. Yoon W-J, Jung K-Y, Liu J, Duraisamy T, Revur R, Teixeira FL, Sengupta S, Berger PR (2009) Efficient poly(3-hexylthiophene)-fullerene derivative bulk heterojunction photovoltaic devices using unique self-assembled layer of Ag nanoparticles with controllable particle-to-particle spacing. In: 2009 34th Ieee Photovoltaic Specialists Conference, vols 1–3. IEEE Photovoltaic Specialists Conference. IEEE, New York, pp 2065–2068
22. Zou SL, Zhao L, Schatz GC (2003) Extinction spectra of silver nanoparticle arrays. In: Halas NJ (ed) Plasmonics: Metallic Nanostructures and Their Optical Properties, vol 5221. Proceedings of the Society of Photo-Optical Instrumentation Engineers (Spie). Spie-Int Soc Optical Engineering, Bellingham, pp 174–181
23. Weeber J-C, Girard C, Krenn JR, Dereux A, Goudonnet J-P (1999) Near-field optical properties of localized plasmons around lithographically designed nanostructures. J Appl Phys 86(5):2576–2583. doi:10.1063/1.371095
24. Yee KS (1966) Numerical solution of initial boundary value problems involving Maxwell's equations in isotropic media. IEEE Trans Antennas Propag AP14 (3):302–307
25. Teixeira FL (2008) Time-domain finite-difference and finite-element methods for Maxwell equations in complex media. IEEE Trans Antennas Propag 56(8):2150–2166. doi:10.1109/tap.2008.926767
26. Berenger JP (1994) A perfectly matched layer for the absorption of electromagnetic-waves. J Comput Phys 114 (2):185-200. doi:10.1006/jcph.1994.1159
27. Teixeira FL, Chew WC (1998) A general approach to extend Berenger's absorbing boundary condition to anisotropic and dispersive media. IEEE Trans Antennas Propag 46(9):1386–1387. doi:10.1109/8.719984
28. Teixeira FL, Chew WC (2000) Complex space approach to perfectly matched layers: a review and some new developments. Int J Numer Modell Electron Networks Devices Fields 13(5):441–455. doi:10.1002/1099-1204(200009/10)13:5<441::aid-jnm376>3.0.co;2-j
29. Atwater HA, Polman A (2010) Plasmonics for improved photovoltaic devices. [Erratum to document cited in CA152:315599]. Nat Mater 9(10):865. doi:10.1038/nmat2866
30. Atwater HA, Polman A (2010) Plasmonics for improved photovoltaic devices. Nat Mater 9(3):205–213. doi:10.1038/nmat2629
31. Hoevel H, Fritz S, Hilger A, Kreibig U, Vollmer M (1993) Width of cluster plasmon resonances: bulk dielectric functions and chemical interface damping. Phys Rev B Condens Matter 48(24):18178–18188